ACS OMEGA

http://pubs.acs.org/journal/acsodf

Article

Theoretical Study of the Kinetics of the Gas-Phase Reaction between Phenyl and Amino Radicals

Tien V. Pham,* Hoang T. Tue Trang, Trinh Le Huyen, and Tue Ngoc Nguyen

Cite This: *ACS Omega* 2020, 5, 1277−1286

Read Online

ACCESS | Metrics & More | Article Recommendations | Supporting Information

ABSTRACT: The potential energy surface (PES) of the C_6H_5 + NH_2 reaction has been investigated by using ab initio CCSD(T)//B3LYP/6-311++G(3df,2p) calculations. The conventional transition-state theory (TST) and the variable reaction coordinate-TST (VRC-TST) have been used to predict the rate constants for the channels possessing tight and barrierless transition states, respectively. The Rice−Ramsperger−Kassel−Marcus/Master equation (RRKM/ME) theory has been utilized to determine the pressure-dependent rate constants for these reactions. The PES shows that the reaction begins with an exothermic barrierless addition of NH_2 to C_6H_5 producing the vital intermediate state, namely, aniline ($C_6H_5NH_2$, IS1). Once IS1 is generated, it can further isomerize to various intermediate states, which can give rise to different products, including PR4 (4,5,6-trihydro-1-amino phenyl + H_2), PR5 (3,4,5,6-tetrahydro phenyl + NH_3), PR6 (2,3,5,6-tetrahydro-1-imidogen phenyl + H_2), PR9 (3,4,5,6-tetrahydro-1-imidogen phenyl + H_2), and PR10 (2,5,6-trihydro-1-amino phenyl + H_2), of which the most stable product, PR5, was formed by the most favorable channel going through the two advantageous transition states T1/11 (−28.9 kcal/mol) and T11P5 (−21.5 kcal/mol). The calculated rate constants for the low-energy channel, 1.37×10^{-9} and 2.16×10^{-11} cm^3 $molecule^{-1}$ s^{-1} at T = 300, P = 1 Torr and T = 2000 K, P = 760 Torr, respectively, show that the title reaction is almost pressure- and temperature-dependent. The negative temperature-dependent rate coefficients can be expressed in the modified Arrhenius form of $k_1 = 8.54 \times 10^{13}\ T^{-7.20}$ exp (−7.07 kcal·mol^{-1}/RT) and $k_2 = 2.42 \times 10^{15}\ T^{-7.61}$ exp (−7.75 kcal·mol^{-1}/RT) at 1 and 10 Torr, respectively, and in the temperature range of 300−2000 K. The forward and reverse rate coefficients as well as the high-pressure equilibrium constants of the C_6H_5 + NH_2 ↔ IS1 process were also predicted; their values revealed that its kinetics do not depend on pressure at low temperature but strongly depend on pressure at high temperature. Moreover, the predicted formation enthalpies of reactants and the enthalpy changes of some channels are in good agreement with the experimental results.

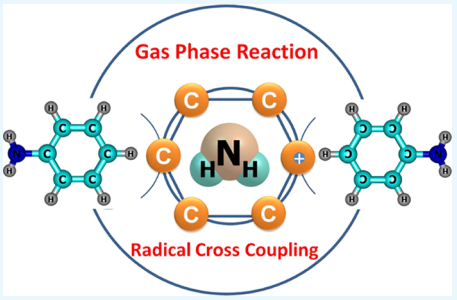

1. INTRODUCTION

The phenyl radical, C_6H_5, has been known to play a vital role in the pyrolysis and oxidation of polycyclic aromatic hydrocarbons (PAHs), as well as in soot formation in combustion chemistry for many years.[1−5] In extraterrestrial environments, some species such as benzene, phenyl radical, and cyclo-C_5H_5 radicals have been considered to be crucial reaction intermediates in the formation of PAHs, as shown in several studies.[1−3] In combustion conditions, similarly, the formation of PAHs and soot particles is usually derived from an aromatic compound like a benzene molecule or a phenyl radical.[6] Because of the important function of C_6H_5 as mentioned above, there have been theoretical and experimental investigations into its reaction with closed- and/or open-shell species such as C_2H_2, C_3H_4, CH_4, NO, O_2, CH_3, etc. in different environments including the circumstellar envelopes of carbon-rich stars, the interstellar medium, and the combustion processes.[7−25]

Glassman[25] and Bittner et al.[13] reported that, at high temperatures, blocks of soot particles in the combustion of hydrocarbons can be obtained via the two reactions of C_6H_5 with C_2H_2 and O_2, in which, if the C_6H_5 + nC_2H_2 → PAHs reaction shows the polymerization process of phenyl radical, the C_6H_5 + O_2 reaction shows the oxidization of C_6H_5. The mechanisms, rate constants, and branching ratios of these two reactions under distinct temperature and pressure conditions were also investigated sufficiently to specify the quantity of soot formed in combustion. Frenklach et al.[4,5] proposed a sequential-addition mechanism of C_2H_2 to the phenyl radical to yield PAHs, which is the best chosen synthetic way in interstellar and combustion chemistry instead of the old-fashioned means based on the combination of C_3H_3 and C_3H_2 or C_2H_2 and C_4H_x considered by most authors.[26−30] The other reaction series involved in phenyl radical including C_6H_5 + H_2, C_6H_5 + CH_3, C_6H_5 + CH_4, C_6H_5 + NO, and C_6H_5 + CO have been carried out theoretically and experimentally,[30−37] which indicated that these reactions occurred quickly in combustion conditions.

Received: November 20, 2019
Accepted: December 27, 2019
Published: January 9, 2020

https://dx.doi.org/10.1021/acsomega.9b03967
ACS Omega 2020, 5, 1277−1286

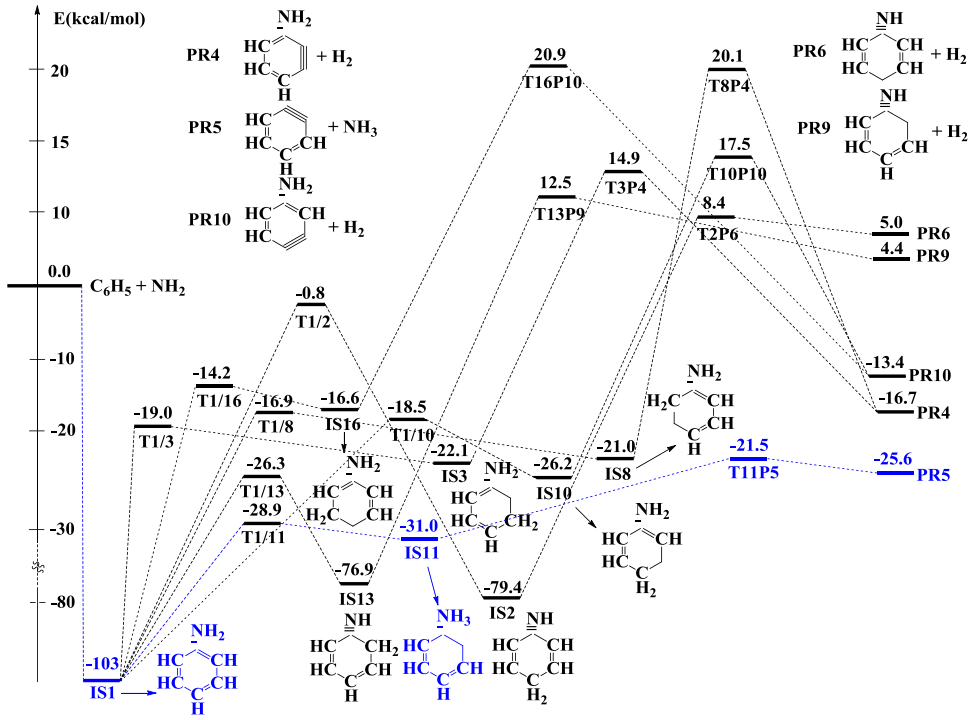

Figure 1. Simplified potential energy surface (PES) for the C_6H_5 + NH_2 reaction calculated at the CCSD(T)//B3LYP/6-311++G(3df,2p) + zero-point vibrational energies (ZPVE) level of theory (energies are in kcal/mol).

As far as we are aware, the mechanism and kinetics of the reaction between the C_6H_5 radical and the NH_2 radical, at various temperatures and pressures, have not yet been investigated both theoretically and experimentally. Due to the lack of such qualitative and quantitative data, the reaction of C_6H_5 with NH_2 should be researched fully and carefully. Therefore, the PES characterizing the C_6H_5 + NH_2 reaction has been theoretically figured out in the present work. This reaction was not suggested earlier as a possible source of PAH precursors, but it is an appropriate representative of the layer of reactions of aromatic molecules with species with a single electron. The PES of this reaction reveals that the energetically most favorable reaction path yields 3,4,5,6-tetrahydro phenyl and that this advantageous path is straightforward to approach with an activated intermediate generated initially, even at very low temperatures and/or pressures. This work, subsequently, has focused on the rate constants of the energetically low-lying channel proceeding over this PES by theoretical−kinetic analysis. The thermochemical parameters denoted as enthalpy, Gibbs free energy, and entropy changes of some main channels involved in the system were also measured and were compared to experimental data to determine the validity of the method used in this calculation.

2. COMPUTATIONAL METHODS

The density functional theory (DFT) with the common B3LYP[38−40] and M06-2X[41−43] functionals in conjunction with the 6-311++G(3df,2p)[44] and aug-cc-pVTZ[45−47] basis sets, respectively, was used to figure out the mechanism for the title reaction. In this work, the geometries optimized by the B3LYP/6-311++G(3df,2p) method were utilized for the establishment of the PES and the kinetic prediction. The correlative parameters, including vibrational frequencies, moments of inertia, and zero-point vibrational energies (ZPVE), were obtained using the same method. All species in the system were classified based on their vibrational analysis, of which the local minima such as reactants, intermediates, and products all have positive frequencies, while each saddle point like a transition state contains only one unreal frequency. The intrinsic reaction coordinate (IRC)[48,49] predictions were employed to verify the validity of transition states. The B3LYP/6-311++G(3df,2p) relative energies of all points were then refined by the single-point energy calculations using the CCSD(T)/6-311++G(3df,2p)[50] + ZPVEs level of theory. The ZPVE values were corrected by a factor of 0.97.[51] The Gaussian 16 software package[52] was utilized to optimize and compute single-point energies for all species in this system.

The rate coefficients for the energetically low-lying channel have been predicted by employing the Variflex code[53] and the Multiwell code[54] depending on the transition-state theory (TST),[55] variable reaction coordinate-TST (VRC-TST),[56,57] and the Rice−Ramsperger−Kassel−Marcus (RRKM) theory[58] with Eckart tunneling corrections.[59] The sum and density of state in the kinetic model were estimated from the input data file containing the energy barriers of the reaction path and the species' parameters mentioned above. The master equation[60] involving multistep vibrational energy transfer for the $C_6H_5NH_2$ excited intermediate state was solved to obtain the pressure- and temperature-dependent rate constants using the energy-dependent microcanonical RRKM statistical rate constants, $k(E)$.

The collisional frequency of the bath gas (Ar in the present work) and the intermediate states have been taken from references. In the present study, the values of Lennard-Jones (L-J) of Ar are ε/k_B = 113.50 K and σ = 3.465 Å,[61] whereas the values of the intermediates are σ = 5.923 Å and ε = 407.8 K.[62] The average energy transferred per collision, $\langle \Delta E \rangle_{down}$ = 400 cm^{-1}, was used for the standard form of the "exponential down" model.[63] A brief discussion of the rate constant prediction is presented in Supporting Information (SI).

https://dx.doi.org/10.1021/acsomega.9b03967
ACS Omega 2020, 5, 1277−1286

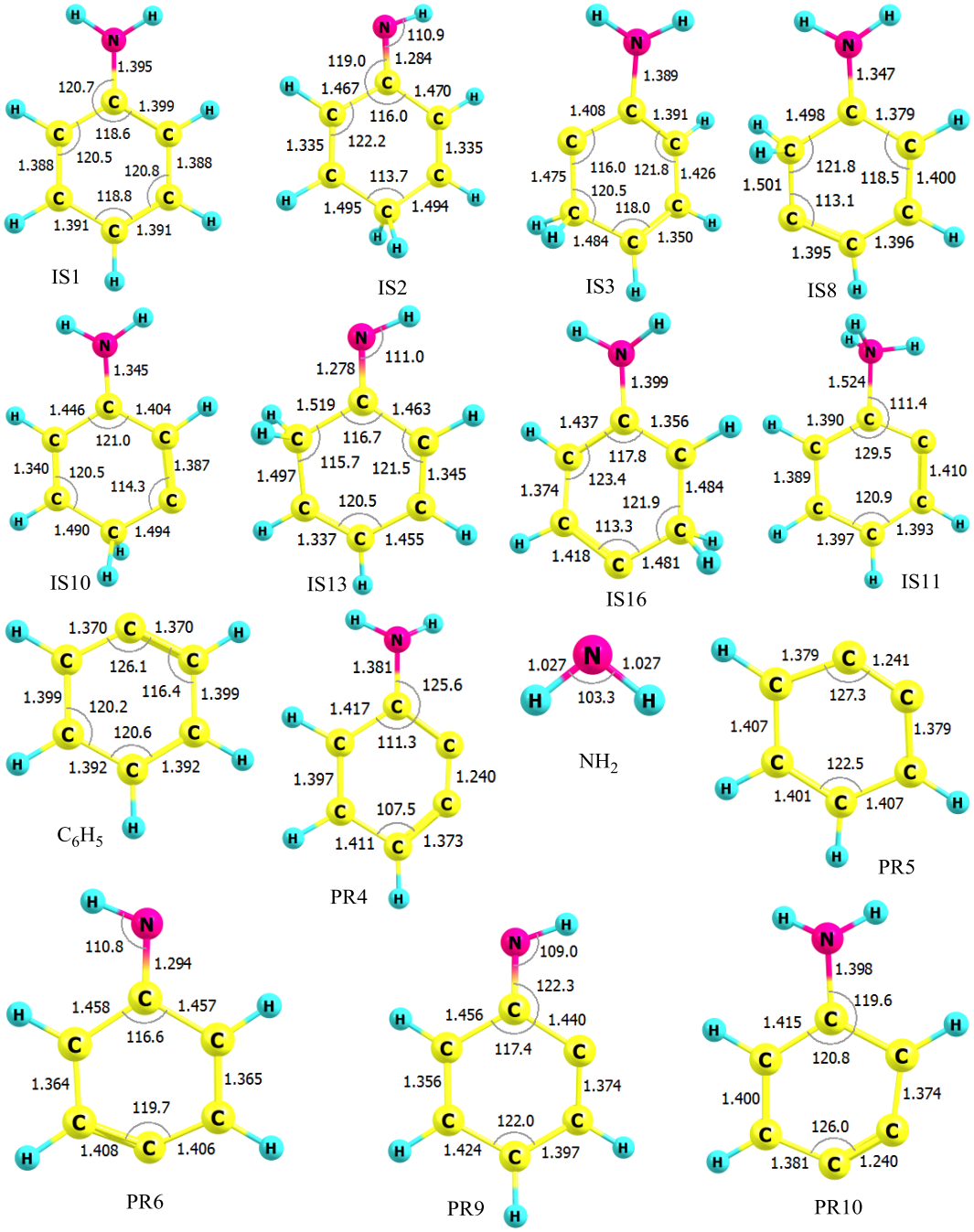

Figure 2. Geometries of the intermediate states, complexes, reactants, and products optimized at the B3LYP/6-311++G(3df,2p) level (bond lengths are in angstrom and bond angles are in degrees).

3. RESULTS AND DISCUSSION

3.1. Potential Energy Surface and Reaction Mechanism. The detailed PES characterized at the (U)CCSD(T)//B3LYP/6-311++G(3df,2p) level is indicated in Figure S1 (see the SI), while the simplified PES containing the significant channels is presented in Figure 1 of this work. The geometric structures of all species for the C_6H_5 + NH_2 reaction were optimized at the B3LYP/6-311++G(3df,2p) level and are shown in Figures 2 and 3 as well as in Figure S2 of the SI file.

The relative energies for all species related to Figure 1 at various levels of theory are shown in Table 1. The calculated heats of formation and heats of reaction in the C_6H_5 + NH_2 system are compared to the experimental data and presented in Table 2. The harmonic vibrational frequencies and the Cartesian coordinates of the species involved are listed in Tables S1 and S2, respectively. The Gibbs free energies (ΔG) and entropies (ΔS) under the standard condition of all channels are presented in Table S3.

It can be seen from Table 2 that the predicted heats of formation of some species C_6H_5, NH_2, and $C_6H_5NH_2$ at the CCSD(T)//B3LYP/6-311++G(3df,2p) level of theory are 80.47, 44.05, and 20.26 kcal/mol, respectively, while the values at the CCSD(T)//M06-2×/aug-cc-pVTZ level are 81.82, 42.43, and 20.29 kcal/mol, respectively. These values are in reasonable agreement with the experimental results. Likewise, the heats of several reaction paths creating IS1, PR4, PR5, PR6,

https://dx.doi.org/10.1021/acsomega.9b03967
ACS Omega 2020, 5, 1277−1286

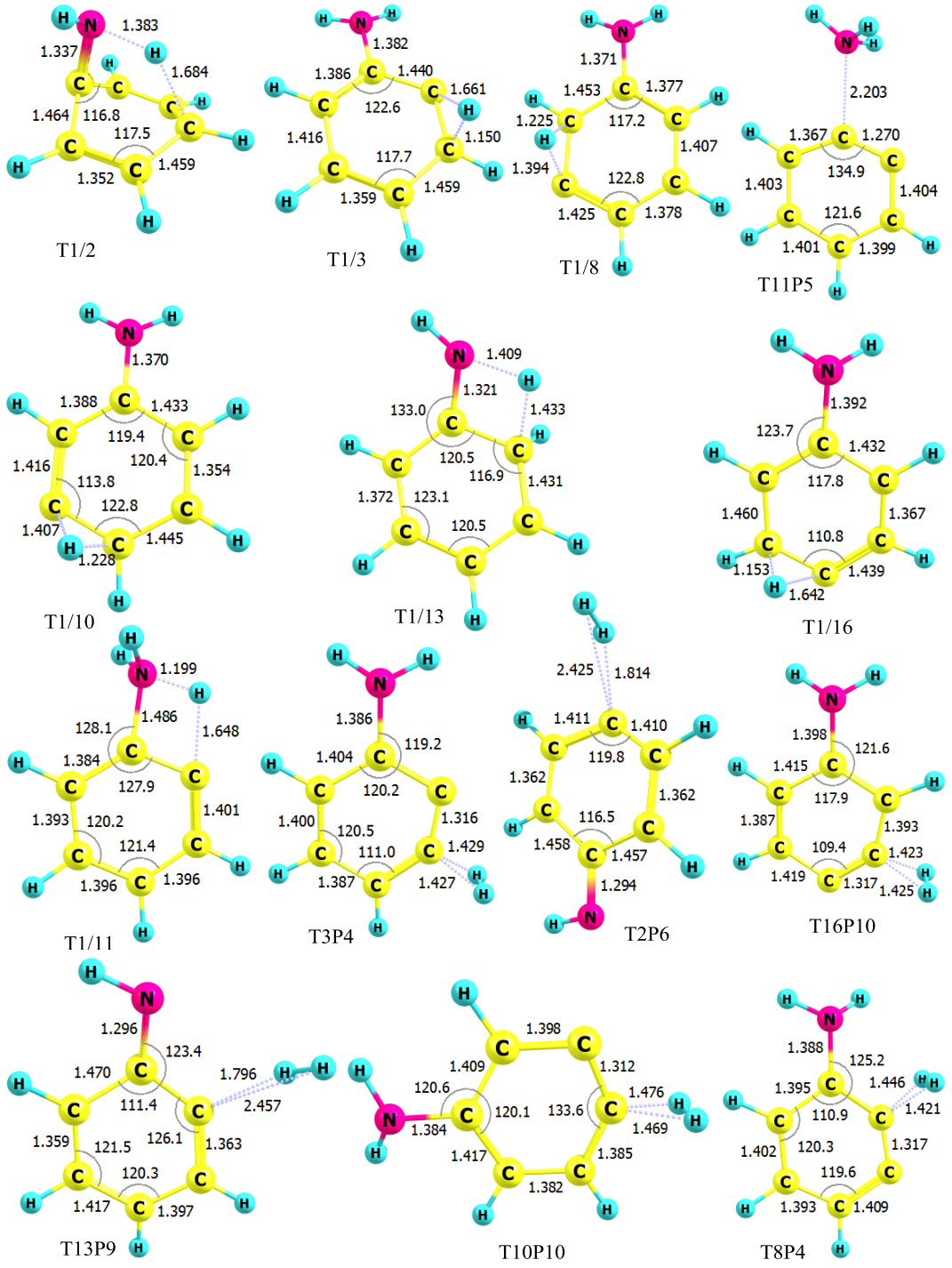

Figure 3. Geometries of the main transition states optimized at the B3LYP/6-311++G(3df,2p) level (bond lengths are in angstrom and bond angles are in degrees).

PR9, and PR10 at the CCSD(T)//B3LYP/6-311++G(3df,2p) level of theory are −104.26, −16.13, −25.53, 5.35, 4.89, and −12.74 kcal/mol, respectively. Those values at the CCSD-(T)//M06-2×/aug-cc-pVTZ level are −103.96, −14.34, −25.23, 7.71, 7.27, and −10.93 kcal/mol, respectively. Both sets of results are in agreement with available experimental data. In addition, the bond-dissociation energy for the $C_6H_5NH_2 \rightarrow C_6H_5 + NH_2$ process calculated in this work based on the heats of formation of C_6H_5, NH_2, and $C_6H_5NH_2$ is 104.26 kcal/mol at the CCSD(T)//B3LYP/6-311++G-(3df,2p) level, which is in excellent agreement with the experimental value, 104.21 ± 0.38 kcal/mol (ref from NIST, webbook.nist.gov).

As shown in Figures 1 and S1, the first intermediate IS1 located at −103 kcal/mol is the result of the additional reaction between two reactants, which takes place without a well-defined transition state. From IS1, there are various different subchannels created to yield other intermediates or products (see Figure S1), of which some subchannels can be ignored because they proceed via high-energy barriers of over 18 kcal/mol. In Figure 1, hence, we only consider seven potential channels possessing low transition states. Those

https://dx.doi.org/10.1021/acsomega.9b03967
ACS Omega 2020, 5, 1277−1286

Table 1. Theoretical Prediction of the Relative Energies, ΔE (kcal/mol), for the Species Involved in Figure 1 of the C_6H_5 + NH_2 Reaction at Two Different Levels

	relative energies (kcal/mol)	
species	CCSD(T)/aug-cc-pVTZ//M06-2×/aug-cc-pVTZ	CCSD(T)/6-311++G(3df,2p)//B3LYP/6-311++G(3df,2p)
C_6H_5 + NH_2	0.0	0.0
IS1	−101.4	−103.0
IS2	−77.6	−79.4
IS3	−20.1	−22.1
IS8	−19.6	−21.0
IS10	−24.7	−26.2
IS13	−75.0	−76.9
IS16	−14.7	−16.6
IS11	−29.4	−31.0
T1/2	1.3	−0.8
T1/3	−14.4	−19.0
T1/8	−15.7	−16.9
T1/10	−17.2	−18.5
T1/13	−25.1	−26.3
T1/16	−12.0	−14.2
T1/11	−27.8	−28.9
T11P5	−20.9	−21.5
T2P6	11.3	8.4
T3P4	16.3	14.9
T8P4	21.5	20.1
T10P10	18.8	17.5
T13P9	14.5	12.5
T16P10	22.5	20.9
PR4	−14.0	−16.7
PR5	−24.3	−25.6
PR6	8.2	5.0
PR9	7.7	4.4
PR10	−10.6	−13.4

Table 2. Comparison of the Predicted Heats of Formation ($\Delta_f H°$, in kcal/mol) and Heats of Reaction ($\Delta_r H°$, in kcal/mol) at 298.15 K in This Work with Available Data

	methods		
species/paths	CCSD(T)//M06-2×/aug-cc-pVTZ	CCSD(T)//B3LYP/6-311++G(3df,2p)	experiments
C_6H_5	81.82	80.47	80.54 ± 0.60[65] 80.62 ± 0.14[66]
NH_2	42.43	44.05	44.5 ± 0.24[a] 45.5[67]
$C_6H_5NH_2$	20.29	20.26	20.8 ± 0.24[68] 19.69[69] 19.88[70] 19.36 ± 0.72[71] 20.41[72]
C_6H_5 + NH_2 → IS1 ($C_6H_5NH_2$)	−103.96	−104.26	−104.21 ± 0.38[a]
C_6H_5 + NH_2 → PR4	−14.34	−16.13	
C_6H_5 + NH_2 → PR5	−25.23	−25.53	−25.79 ± 1.54[a]
C_6H_5 + NH_2 → PR6	7.71	5.35	
C_6H_5 + NH_2 → PR9	7.27	4.89	
C_6H_5 + NH_2 → PR10	−10.93	−12.74	

[a]Ref from NIST (webbook.nist.gov).

channels go through two tight transition states before reaching the products. The first path proceeds via transition states, T1/11 (−28.9 kcal/mol) and T11P5 (−21.5 kcal/mol), and stops at the product PR5 [C_6H_4 (*o*-benzyne) + NH_3] at −25.6 kcal/mol. The T1/11 transition state connecting IS1 with IS11 (−31 kcal/mol) has only one imaginary frequency of 1288*i* corresponding to an H-shift from the ortho position to the $-NH_2$ group with a distance of 1.648 and 1.199 Å, respectively, which makes the C−NH_2 bond elongate from 1.395 Å in IS1 to 1.486 Å in IS11. Whereas the ∠C2C1C2 angle increases nearly 11 °C, the ∠C1C2C3 angle decreases about 8 °C, in which C2 and C3 denote the carbon atoms at ortho and meta positions, respectively. It is worth noting that the structure of T1/11 has been confirmed by IRC analysis

https://dx.doi.org/10.1021/acsomega.9b03967
ACS Omega 2020, 5, 1277−1286

with the B3LYP/6-311++G(3df,2p) method along the forward direction from IS1 to IS11 as well as the reverse direction from IS11 back to IS1 (see Figure S3). These results reveal that T1/11 is the accurate transition state connecting IS1 and IS11. Similarly, the T11P5 transition state connecting IS11 to the product PR5 also has only one imaginary frequency of 131.9617*i* relating to the dissociation of the C−NH_3 bonding with a distance of 2.203 Å. It can be seen from Figure 1 that the reaction path generating PR5 is the most favorable channel in terms of energy compared to the others. Therefore, the process from the reactants to PR5 contributes mainly to the overall rate constant of the title reaction. The second path producing the product PR9 passes two transition states T1/13 and T13P9, for which the transition state T1/13 connecting IS1 with IS13 shows a transfer of a H atom from the NH_2 group to the CH group at the ortho location. It may be noted that IS13 can be easily produced because T1/13 lies at a fair depth below the reactants about 26 kcal/mol; thus, an extremely enormous exothermicity from the first step (reactants to IS1) can help IS1 easily cross T1/13. Once IS13 is formed, it can be converted to product PR9 via T13P9; this process needs plenty of energy to pass over the high barrier of nearly 90 kcal/mol. In addition, the reaction path giving product PR9 is an exothermic channel with 4.4 kcal/mol. This product, hence, is guessed hardly to appear at room temperature. The product PR4 can be established from two different paths; the first path goes through two transition states such as T1/3 and T3P4, while the second path occurs via T1/8 and T8P4. Both channels effortlessly pass transition states T1/3 (−19 kcal/mol) and T1/8 (−16.9 kcal/mol) at the early stages, but it is difficult to overcome high-energy barriers T3P4 (∼15 kcal/mol) and T8P4 (∼20 kcal/mol) at the later stages. Of these, T1/3 and T1/8 show a 2,3-H-shift and a 3,2-H-shift, respectively, whereas T3P4 and T8P4 present two H_2-abstractions from para and ortho positions, respectively. Therefore, PR4 is also considered to be difficult to form in normal conditions even though the formation of PR4 from these two channels is exothermic by 16.7 kcal/mol. Similarly, the product PR10 was also created by two different pathways: one passes through the transition states T1/10 and T10P10, while the other one proceeds via the transition states T1/16 and T16P10. Figure 1 shows that if T1/10 describes a H-shift between meta and para locations yielding IS10 (−26.2 kcal/mol), T1/16 shows a reverse transfer of a H atom from para to meta positions forming the intermediate state IS16 lying under the reactants by 16.6 kcal/mol. The relative energy of T16P10 in the second channel is higher than the one of T10P10 in the first channel by about 3 kcal/mol. The second channel is thus predicted to donate less consideration to the PR10 product. However, both TSs possess very high-energy barriers (see Figure 1); thus, the PR10 product is predicted to be difficult to form in the low-temperature region. The overall exothermicity of the reaction path resulting in the PR10 product is 13.4 kcal/mol. It is worth noting that the PR5 product is the most stable one compared to the others on the whole PES. Last but not least, the IS1 intermediate state formed at the first step can also isomerize to the IS2 isomer, which is located at −79.4 kcal/mol, via T1/2 with a 102 kcal/mol energy barrier. The geometry of T1/2 in Figure 3 shows a very far H-shift from the NH_2 group to the *para*-C atom at distances of 1.383 and 1.684 Å, respectively, which makes this process lose more energy than others. The bimolecular products C_6H_4NH + H_2 (denoted as PR6) with 5.0 kcal/mol of endothermicity can be generated by eliminating a hydrogen molecule out of the IS2 geometry when it proceeds via the T2P6 transition state lying 8.4 kcal/mol above the entry point.

Briefly, many various products can be formed through the addition channel, as shown in Figure 1, in which, the channel going via transition structures T1/11 (−28.9 kcal/mol) and T11P5 (−21.5 kcal/mol) producing PR5 is found to be dominant, while the others proceeding via T1/3 (−19 kcal/mol), T1/10 (−18.5 kcal/mol), T1/8 (−16.9 kcal/mol), T1/16 (−14.2 kcal/mol), and T1/2 (−0.8 kcal/mol) forming PR4, PR6, PR9, and PR10 are less favorable. Accordingly, the dominant reaction path yielding PR5 is expected to be kinetically advantageous.

3.2. Rate Constant Calculations. The rate constants for the title reaction have been calculated based on the main PES shown in Figure 1. Many channels of the reaction, as discussed above, can be overlooked due to their too high-energy barriers. Only one reaction path proceeding via the two transition states T1/11 and T11P5 giving rise to the product PR5 has been considered. For this reason, the rate constants of the C_6H_5 + NH_2 reaction have been calculated relying on the channel as shown below

$$C_6H_5 + NH_2 \rightarrow C_6H_5NH_2(IS1) \rightarrow T1/11 \rightarrow IS11 \rightarrow T11P5 \rightarrow PR5$$

The rate constants of the barrierless process, C_6H_5 + NH_2 → IS1, have been determined by using the VRC-TST procedure with the Variflex code.[53] The treatment of microvariational RRKM and the Morse functional model[64] have also been utilized to estimate the minimum energy path (MEP) curve presented as follows

$$V(r) = D_e[1 - \exp(-\beta(r-r_e))]^2$$

where D_e is the dissociation energy excluding the zero-point energy; r and r_e are the reaction coordinate and equilibrium value of r; and β is the constant derived from the fitted equation to the estimated MEP.

The computed barrierless rate coefficients under the conditions of this study are shown in Table S4 in the SI file and are plotted in Figure 4. It is shown that the rate constants, at low temperatures ($T \leq 600$ K), slightly increase and do not depend on pressures. At high temperatures ($T \geq 700$, 800,

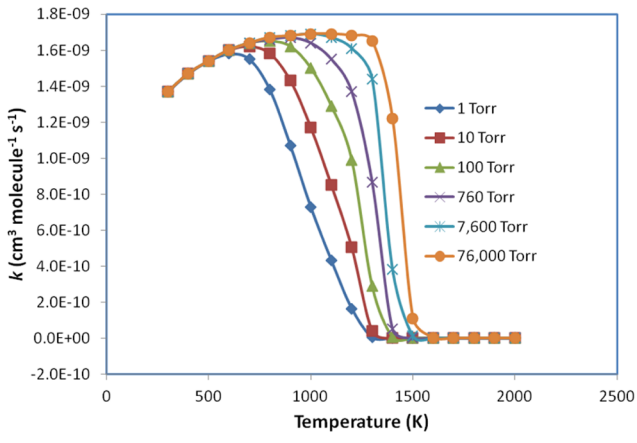

Figure 4. Plots of predicted rate constants for the C_6H_5 + NH_2 → $C_6H_5NH_2$ process in the temperature range of 300−2000 K at various pressures of 1−76 000 Torr Ar.

https://dx.doi.org/10.1021/acsomega.9b03967
ACS Omega 2020, 5, 1277−1286

900, 1000, 1100, and 1200 K at P = 1, 10, 100, 760, 7600, and 76 000 Torr, respectively), those values sharply decrease and strongly depend on pressure.

The rate constants for the reverse process, $C_6H_5NH_2 \rightarrow C_6H_5 + NH_2$, have also been computed with the RRKM theory under varying T, P conditions. Similar to the forward process, this channel takes place without a well-defined transition state; its rate constants can thus be predicted with the VRC-TST approach based on the maximum $\Delta G^{\ddagger}$ criterion. The rate constants predicted by solving the master equation using the Multiwell code[54] for various Ar pressures between 1 and 76 000 Torr in the temperature range of 300−2000 K are given in Table S5 and Figure 5. As can be seen, the decomposition

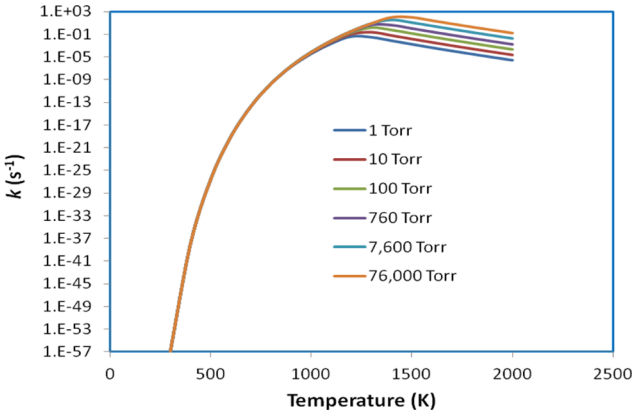

Figure 5. Plots of predicted rate constants for the decomposition process, $C_6H_5NH_2 \rightarrow C_6H_5 + NH_2$, in the temperature range of 300−2000 K at various pressures of 1−76 000 Torr Ar.

rate constants quickly increase in the temperature range of 300 ≤ T ≤ 1100 K and gradually decrease when temperatures surpass over 1200 K (at 1 Torr), 1300 K (at 10, 100, and 760 Torr), and 1400 K (at 7600 and 76 000 Torr). Moreover, the equilibrium constants at the high-pressure limit for the $C_6H_5 + NH_2 \leftrightarrow$ IS1 process have been calculated and are shown in Table S4. These values drop sharply as temperatures increase, e.g., K^{∞}(equiv) = 1.18×10^{48} and 2.74×10^{-16} cm^3 molecule^{-1} at 300 and 2000 K, respectively.

The pressure- and temperature-dependent rate constants, k(T, P), for the $C_6H_5 + NH_2 \rightarrow$ PR5 channel were determined by using the Multiwell program[54] with the use of the Eckart tunneling effects[59] under the same conditions as above. The calculated results are presented in Table S6 and are plotted in Figure 6. The modified Arrhenius equation with three parameters adequately describes those data in the temperature range of 300−2000 K at various pressures of Ar and can be given (in units of cm^3 molecule^{-1} s^{-1}) as follows

$$k_1 = 8.54 \times 10^{13}\, T^{-7.20} \exp\left(-7.07\ \text{kcal·mol}^{-1}/RT\right) \text{ at 1 Torr}$$

$$k_2 = 2.42 \times 10^{15}\, T^{-7.61} \exp\left(-7.75\ \text{kcal·mol}^{-1}/RT\right) \text{ at 10 Torr}$$

$$k_3 = 2.66 \times 10^{16}\, T^{-7.89} \exp\left(-8.28\ \text{kcal·mol}^{-1}/RT\right) \text{ at 100 Torr}$$

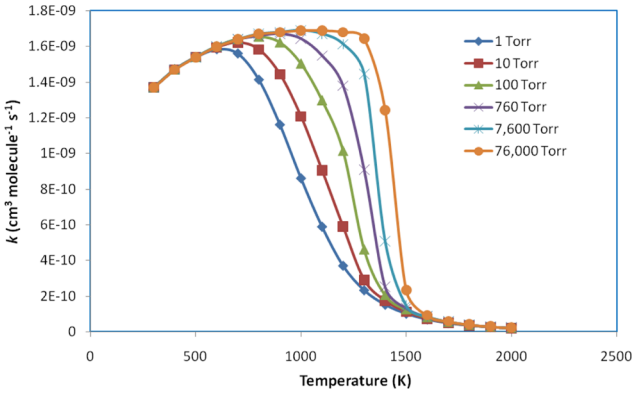

Figure 6. Plots of predicted rate constants for the $C_6H_5 + NH_2 \rightarrow$ PR5 reaction in the temperature range of 300−2000 K at various pressures of 1−76 000 Torr Ar.

$$k_4 = 8.98 \times 10^{16}\, T^{-8.03} \exp\left(-8.59\ \text{kcal·mol}^{-1}/RT\right) \text{ at 760 Torr}$$

$$k_5 = 1.30 \times 10^{17}\, T^{-8.06} \exp\left(-8.76\ \text{kcal·mol}^{-1}/RT\right) \text{ at 7600 Torr}$$

$$k_6 = 7.76 \times 10^{16}\, T^{-8.79} \exp\left(-8.79\ \text{kcal·mol}^{-1}/RT\right) \text{ at 76 000 Torr}$$

It is observed that the rate constants for the designated reaction channel shown in Table S6 and Figure 6 tend to gradually increase in the low-temperature regions ($T \leq$ 600, 700, 800, 900, 1000, and 1100 for k_1, k_2, k_3, k_4, k_5, and k_6, respectively). For instance, the rate constants at T = 300, P = 1 Torr and T = 600 K, P = 1 Torr are 1.37×10^{-9} and 1.58×10^{-9} cm^3 molecule^{-1} s^{-1}, respectively. As the temperature increases (T > 600, 700, 800, 900, 1000, and 1100 at 1, 10, 100, 760, 7600, and 76 000 Torr, respectively), the rate coefficients sharply decrease, e.g., the rate constants are 1.67×10^{-9} and 2.16×10^{-11} cm^3 molecule^{-1} s^{-1} at T = 900 K, P = 760 Torr and T = 2000 K, P = 760 Torr, respectively. In addition, it is found that the effect of pressure on the rate constants is negligible at low and high temperatures (e.g., $T \leq$ 600 and T > 1700 K, cf. Figure 6) owing to higher-energy decomposition processes and indirect isomerization/decomposition processes. In the temperature range of 600−1700 K, the predicted rate coefficients positively depend on pressure (e.g., at the same temperature, T = 1000 K, $k_1 = 8.61 \times 10^{-10}$ cm^3 molecule^{-1} s^{-1} at P = 1 Torr, while $k_6 = 1.69 \times 10^{-9}$ cm^3 molecule^{-1} s^{-1} at P = 76 000 Torr).

The rate coefficients at high-pressure limit, $k^{\infty}(T)$, were also predicted and are listed in Table S6 in the temperature range of 300 ≤ T ≤ 2000 K. In this situation, likewise, the rate constants slightly increase with an increase of temperature from 300 to 1100 K and gradually decrease at temperatures above 1200 K. At low temperature ($T \leq$ 600 K), as discussed above, $k^{\infty}(T)$ is equal to k_i (i = 1−6) (e.g., 1.37×10^{-9} at T = 300 K or 1.60×10^{-9} cm^3 molecule^{-1} s^{-1} at T = 600 K), while in the high-temperature region ($T \geq$ 1500 K), the high-pressure limit rate constant is much greater than the others in the range of pressure P = 1−76 000 Torr (e.g., at T = 2000 K, $k_1 = 2.10 \times 10^{-11}$ vs $k^{\infty}(T) = 1.52 \times 10^{-9}$ cm^3 molecule^{-1} s^{-1}), as shown in Table S6.

https://dx.doi.org/10.1021/acsomega.9b03967
ACS Omega 2020, 5, 1277−1286

The effects of the error margins of energy about ± 2 kcal/mol estimated by the CCSD(T)//B3LYP/6-311++G(3df,2p) method on the rate constants for the formation and dissociation of $C_6H_5NH_2$ were also considered. The computed values in various conditions are presented in Figures S7−S10 in the SI file. These results show that the rate constants for the formation of $C_6H_5NH_2$ remain almost unchanged at low temperatures ($T \leq 1200$ K) but change quickly at high temperatures ($T \geq 1300$ K). At 2000 K and 760 Torr Ar, the value associated with a −101 kcal/mol energy of $C_6H_5NH_2$ is 3.01×10^{-19} cm^3 molecule^{-1} s^{-1}, which is 4.97×10^{-19} cm^3 molecule^{-1} s^{-1} at the energy of −103 kcal/mol, while the value at −105 kcal/mol energy increases by nearly 2 orders of magnitude in going to 1.57×10^{-17} cm^3 molecule^{-1} s^{-1} (see Tables S4, S7, and S9). In contrast, at low temperatures ($T \leq 1100$ K), the rate constants for the decomposition of $C_6H_5NH_2 \rightarrow C_6H_5 + NH_2$ decrease according to the reduction of the C_6H_5−NH_2-binding energy (BDE). However, at high temperatures ($T \geq 1400$ K), those values increase slightly when the BDE increases from 101 to 105 kcal/mol, as shown in Tables S5, S8, and S10.

4. CONCLUSIONS

The mechanism and kinetics, as well as thermodynamics of the $C_6H_5 + NH_2$ reaction, have been investigated based on the quantum chemical theory. The B3LYP method in conjunction with the basic set 6-311++G(3df,2p) has been employed to optimize for the species related in this reaction, such as reactants, intermediate states, transition states, and products. The high method CCSD(T) with the same basic set above has also been utilized to calculate single-point energies for all species on the potential energy surface.

The mechanism of the title reaction at the entrance channel takes place as the additional style without a well-defined transition state to form the stable intermediate $C_6H_5NH_2$ standing at 103 kcal/mol below the reactants. The most dominant channel connecting IS1 with product PR5 proceeds via two different transition states T1/11 and T11P5 lying 28.9 and 21.5 kcal/mol under the reactants, respectively.

The predicted heats of formation of several species (C_6H_5, NH_2, $C_6H_5NH_2$), as well as the heats of reaction of some reaction paths producing IS1, PR4, PR5, PR6, PR9, and PR10 at the CCSD(T)//B3LYP/6-311++G(3df,2p) and CCSD(T)//M06-2×/aug-cc-pVTZ levels of theory are in agreement with the available experimental data. Those results confirm that the methods used in this work are reliable and the calculated energies can be utilized to compute rate constants for the title reaction.

The predicted rate coefficients for the $C_6H_5 + NH_2 \rightarrow$ PR5 channel in the pressure and temperature ranges of 1−76 000 Torr and 300−2000 K, respectively, reveal that its kinetics strongly depends on pressure and temperature, i.e., the rate constants increase at low temperature and decrease at high temperature. The association and dissociation rate constants of the barrierless processes, $C_6H_5 + NH_2 \rightarrow C_6H_5NH_2$ and $C_6H_5NH_2 \rightarrow C_6H_5 + NH_2$, respectively, were nearly independent of pressure at a low temperature and strongly dependent on pressure at a high temperature. Observation of the $C_6H_5 + NH_2 = C_6H_5NH_2$ process showed that there was a large negative temperature dependence of the high-pressure limit equilibrium constants. The effects of the error margins of the energy on the rate constants for the formation and dissociation of $C_6H_5NH_2$ were also considered. The results show that the rate constants for the formation of $C_6H_5NH_2$ remain almost unchanged at low temperatures but change quickly at high temperatures. In contrast, at low temperatures, the rate constants for the $C_6H_5NH_2 \rightarrow C_6H_5 + NH_2$ decomposition decrease according to the reduction of the C_6H_5−NH_2 binding energy but slightly increase at high temperatures.

The results in this study are very important to understand the mechanism and kinetics of the aromatic radical C_6H_5 with some small species such as NH_2, CH_3, etc. They will help researchers in working with various experiments related to this species in the future.

■ ASSOCIATED CONTENT

Supporting Information

The Supporting Information is available free of charge at https://pubs.acs.org/doi/10.1021/acsomega.9b03967.

Variational transition-state theory (VTST) applied for the $C_6H_5 + NH_2 \rightarrow C_6H_5NH_2$ process; frequencies and coordinates of reactants, intermediates, transition states, and products of the $C_6H_5 + NH_2 \rightarrow$ product reaction at the B3LYP/6-311++G(3df,2p) level of theory; Gibbs free energies (ΔG) in kcal/mol using CCSD(T)//B3LYP/6-311++G(3df,2p) and entropies (ΔS) in cal/mols·K using B3LYP/6-311++G(3df,2p); predicted rate constants (cm^3 molecule^{-1} s^{-1}) for the $C_6H_5 + NH_2 \rightarrow C_6H_5NH_2$, $C_6H_5NH_2 \rightarrow C_6H_5 + NH_2$, and $C_6H_5 + NH_2 \rightarrow$ PR5 reactions in the temperature and pressure ranges of 300−2000 K and 1−76 000 Torr, respectively, as well as K_{eq} (cm^3 molecule^{-1}) of the $C_6H_5 + NH_2 \rightarrow C_6H_5NH_2$ process; detailed potential energy surface of the $C_6H_5 + NH_2$ system; geometries of the reactants, intermediate states, transition states, and products optimized at the B3LYP/6-311++G(3df,2p) level; and the IRC profile for the transition state T1/11 calculated at the B3LYP/6-311++G(3df,2p) level of theory (PDF)

■ AUTHOR INFORMATION

Corresponding Author

Tien V. Pham − *Hanoi University of Science and Technology, Hanoi City, Vietnam;* orcid.org/0000-0002-2067-9028; Email: tien.phamvan@hust.edu.vn

Other Authors

Hoang T. Tue Trang − *Hanoi Architectural University, Hanoi City, Vietnam*

Trinh Le Huyen − *National Chiao Tung University, Hsinchu, Taiwan*

Tue Ngoc Nguyen − *Hanoi University of Science and Technology, Hanoi City, Vietnam*

Complete contact information is available at: https://pubs.acs.org/10.1021/acsomega.9b03967

Notes

The authors declare no competing financial interest.

■ ACKNOWLEDGMENTS

The authors thank The Center for Computational Science of Hanoi National University of Education in Vietnam for computational support.

REFERENCES

(1) Cherchneff, I.; Barker, J. R. Polycyclic aromatic hydrocarbons and molecular equilibria in carbon-rich stars. *Astrophys. J.* **1992**, *394*, 703−716.
(2) Messenger, S.; Amari, S.; Gao, X.; Walker, R. M.; Clemett, S. J.; Chillier, X. D. F.; Zare, R. N.; Lewis, R. S. Indigenous polycyclic aromatic hydrocarbons in circumstellar graphite grains from primitive meteorites. *Astrophys. J.* **1998**, *502*, 284−295.
(3) Allain, T.; Sedlmayr, E.; Leach, S. PAHs in circumstellar envelopes. I. Processes affecting PAH formation and growth. *Astron. Astrophys.* **1997**, *323*, 163−176.
(4) Frenklach, M.; Clary, D. W.; Gardiner, W. C.; Stein, S. E. Detailed kinetic modeling of soot formation in shock-tube pyrolysis of acetylene. *Symp. (Int.) Combust.* **1985**, *20*, 887−901.
(5) Kazakov, A.; Frenklach, M. On the relative contribution of acetylene and aromatics to soot particle surface growth. *Combust. Flame* **1998**, *112*, 270−274.
(6) Kern, R. D.; Wu, C. H.; Yong, J. N.; Pamidimukkala, K. M.; Singh, H. J. Correlation of Benzene Production with Soot Yield Measurements As Determined from Fuel Pyrolyses. *Energy Fuels* **1988**, *2*, 454−457.
(7) Abramovich, R. A., Ed. *Reactive Intermediates*; Plenum: New York, 1980.
(8) Almond, M. J., Ed. *Short-lived Molecules*; Ellis Horwood: New York, 1990.
(9) Matthews, H.; Irvine, W. M. The hydrocarbon ring C_3H_2 is ubiquitous in the Galaxy. *Astrophys. J.* **1985**, *298*, L61−L65.
(10) Thaddeus, P.; Vrtilek, J. M.; Gottlieb, C. A. Laboratory and astronomical identification of cyclopropenylidene, C_3H_2. *Astrophys. J.* **1985**, *299*, L63−L66.
(11) Cernicharo, J.; Gottlieb, C. A.; Gue'lin, M.; Killian, T. C.; Paubert, G.; Thaddeus, P.; Vrtilek, J. M. Astronomical detection of H_2CCC. *Astrophys. J.* **1991**, *368*, L39−L41.
(12) Homann, K. Fullerenes and soot formation—new pathways to large particles in flames. *Angew. Chem., Int. Ed.* **1998**, *37*, 2435−2451.
(13) Bittner, J. D.; Howard, J. B. Mechanism of hydrocarbon decay in fuel-rich secondary reaction zones. *Symp. (Int.) Combust.* **1982**, *19*, 211−221.
(14) Castaldi, M. J.; Marinov, N. M.; Melius, C. F.; Huang, J.; Senkan, S. M.; Pitz, W. J.; Westbrook, C. K. Experimental and modeling investigation of aromatic and polycyclic aromatic hydrocarbon formation in a premixed ethylene flame. *Symp. (Int.) Combust.* **1996**, *26*, 693−702.
(15) Bhargava, A.; Westmoreland, P. R. Measured flame structure and kinetics in a fuel-rich ethylene flame. *Combust. Flame* **1998**, *113*, 333−347.
(16) Vereecken, L.; Peeters, J.; Bettinger, H. F.; Kaiser, R. I.; Schleyer, P. V. R.; Schaefer, H. F. Reaction of Phenyl Radicals with Propyne. *J. Am. Chem. Soc.* **2002**, *124*, 2781−2789.
(17) Tokmakov, I. V.; Kim, G. S.; Kislov, V. V.; Mebel, A. M.; Lin, M. C. The Reaction of Phenyl Radical with Molecular Oxygen: A G2M Study of the Potential Energy Surface. *J. Phys. Chem. A* **2005**, *109*, 6114−6127.
(18) Yu, T.; Lin, M. C. Kinetics of the $C_6H_5 + O_2$ reaction at low temperatures. *J. Am. Chem. Soc.* **1994**, *116*, 9571−9576.
(19) Carpenter, B. K. Computational prediction of new mechanisms for the reactions of vinyl and phenyl radicals with molecular oxygen. *J. Am. Chem. Soc.* **1993**, *115*, 9806−9807.
(20) Mebel, A. M.; Lin, M. C. Ab initio molecular orbital calculations of $C_6H_5O_2$ isomers. *J. Am. Chem. Soc.* **1994**, *116*, 9577−9584.
(21) Lin, M. C.; Mebel, A. M. Ab initio molecular orbital study of the $O + C_6H_5O$ reaction. *J. Phys. Org. Chem.* **1995**, *8*, 407−420.
(22) Fadden, M. J.; Barckholtz, C.; Haddad, C. M. Computational study of the unimolecular decomposition pathways of phenylperoxy radical. *J. Phys. Chem. A* **2000**, *104*, 3004−3011.
(23) Fadden, M. J.; Hadad, C. M. Unimolecular decomposition of the 2-oxepinoxy radical: a key seven-membered ring intermediate in the thermal oxidation of benzene. *J. Phys. Chem. A* **2000**, *104*, 8121−8130.
(24) Merle, J. K.; Hadad, C. M. Computational study of the oxygen initiated decomposition of 2-oxepinoxy radical: A key intermediate in the oxidation of benzene. *J. Phys. Chem. A* **2004**, *108*, 8419−8433.
(25) Glassman, I. *Combustion*, 2nd ed.; Academic Press: New York, 1986.
(26) Wu, C. H.; Kern, R. D. Shock-tube study of allene pyrolysis. *J. Phys. Chem. A* **1987**, *91*, 6291−6296.
(27) Alkemade, U.; Homann, K. H. Formation of C_6H_6 isomers by recombination of propynyl in the system sodium vapour/propynylhalide. *Z. Phys. Chem.* **1989**, *161*, 19−34.
(28) Melius, C. F.; Miller, J. A.; Evleth, E. M. Unimolecular reaction mechanisms involving C_3H_4, C_4H_4, and C_6H_6 hydrocarbon species. *Symp. (Int.) Combust.* **1992**, *24*, 621−628.
(29) Morter, C.; Farhat, S.; Adamson, J.; Glass, G.; Curl, R. Rate constant measurement of the recombination reaction $C_3H_3 + C_3H_3$. *J. Phys. Chem. A* **1994**, *98*, 7029−7035.
(30) Miller, J. A.; Volponi, J. V.; Pauwels, J.-F. The effect of allene addition on the structure of a rich C_2H_2/O_2/Ar flame. *Combust. Flame* **1996**, *105*, 451−461.
(31) Mebel, A. M.; Morokuma, K.; Lin, M. C. Modification of the gaussian−2 theoretical model: The use of coupled-cluster energies, density-functional geometries, and frequencies. *J. Chem. Phys.* **1995**, *103*, 7414−7421.
(32) Park, J.; Dyakov, I. V.; Lin, M. C. FTIR and Mass-Spectrometric Measurements of the Rate Constant for the $C_6H_5 + H_2$ Reaction. *J. Phys. Chem. A* **1997**, *101*, 8839−8843.
(33) Tokmakov, I. V.; Park, J.; Gheyas, S.; Lin, M. C. Experimental and Theoretical Studies of the Reaction of the Phenyl Radical with Methane. *J. Phys. Chem. A* **1999**, *103*, 3636−3645.
(34) Tokmakov, I. V.; Park, J.; Gheyas, S.; Lin, M. C. Experimental and Theoretical Studies of the Reaction of the Phenyl Radical with Methane. *J. Phys. Chem. A* **1999**, *103*, 3636−3645.
(35) Park, J.; Gheyas, S. I.; Lin, M. C. Kinetics of C_6H_5 radical reactions with 2-methylpropane, 2,3-dimethylbutane and 2,3,4-trimethylpentane. *Int. J. Chem. Kinet.* **1999**, *31*, 645−653.
(36) Yu, T.; Lin, M. C. Kinetics of the reaction of C_6H_5 with HBr and DBr. *Int. J. Chem. Kinet.* **1994**, *26*, 771−778.
(37) Nam, G. J.; Xia, W.; Park, J.; Lin, M. C. The Reaction of C_6H_5 with CO: Kinetic Measurement and Theoretical Correlation with the Reverse Process. *J. Phys. Chem. A* **2000**, *104*, 1233−1239.
(38) Becke, A. D. Density functional thermochemistry. III. The role of exact exchange. *J. Chem. Phys.* **1993**, *98*, 5648−5652.
(39) Becke, A. D. Density-functional exchange-energy approximation with correct asymptotic-behavior. *Phys. Rev. A* **1988**, *38*, 3098−3010.
(40) Lee, C.; Yang, W.; Parr, R. G. Development of the Colle-Salvetti correlation-energy formula into a functional of the electron density. *Phys. Rev. B* **1988**, *37*, 785−789.
(41) Zhao, Y.; Truhlar, D. G. A New Local Density Functional for Main-Group Thermochemistry, Transition Metal Bonding, Thermochemical Kinetics, and Noncovalent Interactions. *J. Chem. Phys.* **2006**, *125*, No. 194101.
(42) Zhao, Y.; Truhlar, D. G. Density Functional for Spectroscopy: No Long-Range Self-Interaction Error, Good Performance for Rydberg and Charge-Transfer States, and Better Performance on Average than B3LYP for Ground States. *J. Phys. Chem. A* **2006**, *110*, 13126−13130.
(43) Zhao, Y.; Truhlar, D. G. The M06 Suite of Density Functionals for Main Group Thermochemistry, Thermochemical Kinetics, Noncovalent Interactions, Excited States, and Transition Elements. *Theor. Chem. Acc.* **2008**, *120*, 215−241.
(44) Scuseria, G. E.; Janssen, C. L.; Schaefer, H. F., III An efficient reformulation of the closed-shell coupled cluster single and double excitation (CCSD) equations. *J. Chem. Phys.* **1988**, *89*, 7382−7387.
(45) Dunning, T. H., Jr Gaussian Basis Sets for Use in Correlated Molecular Calculations. I. The Atoms Boron through Neon and Hydrogen. *J. Chem. Phys.* **1989**, *90*, 1007−1023.

https://dx.doi.org/10.1021/acsomega.9b03967
ACS Omega 2020, 5, 1277−1286

(46) Peterson, K. A. Chapter 11 Gaussian Basis Sets Exhibiting Systematic Convergence to the Complete Basis Set Limit. *Annu. Rep. Comput. Chem.* **2007**, *3*, 195−206.
(47) Hill, J. G. Gaussian Basis Sets for Molecular Applications. *Int. J. Quantum Chem.* **2013**, *113*, 21−34.
(48) Gonzalez, C.; Schlegel, H. B. An improved algorithm for reaction path following. *J. Chem. Phys.* **1989**, *90*, 2154−2161.
(49) Gonzalez, C.; Schlegel, H. B. Reaction path following in mass-weighted internal coordinates. *J. Chem. Phys.* **1990**, *94*, 5523−5527.
(50) Bartlett, R. J.; Musial, M. Coupled-cluster theory in quantum chemistry. *Rev. Mod. Phys.* **2007**, *79*, 291−352.
(51) Alecu, I. M.; Zheng, J.; Zhao, Y.; Truhlar, D. G. Computational Thermochemistry: Scale Factor Databases and Scale Factors for Vibrational Frequencies Obtained from Electronic Model Chemistries. *J. Chem. Theory Comput.* **2010**, *6*, 2872−2887.
(52) Frisch, M. J.; Trucks, G. W.; Schlegel, H. B.; Scuseria, G. E.; Robb, M. A.; Cheeseman, J. R.; Scalmani, G.; Barone, V.; Petersson, G. A.; Nakatsuji, H.; Li, X.; Caricato, M.; Marenich, A.; Bloino, J.; Janesko, B. G.; Gomperts, R.; Mennucci, B.; Hratchian, H. P.; Ortiz, J. V.; Izmaylov, A. F.; Sonnenberg, J. L.; Williams-Young, D.; Ding, F.; Lipparini, F.; Egidi, F.; Goings, J.; Peng, B.; Petrone, A.; Henderson, T.; Ranasinghe, D.; Zakrzewski, V. G.; Gao, J.; Rega, N.; Zheng, G.; Liang, W.; Hada, M.; Ehara, M.; Toyota, K.; Fukuda, R.; Hasegawa, J.; Ishida, M.; Nakajima, T.; Honda, Y.; Kitao, O.; Nakai, H.; Vreven, T.; Throssell, K.; Montgomery, J. A.; Peralta, J. E.; Ogliaro, F.; Bearpark, M.; Heyd, J. J.; Brothers, E.; Kudin, K. N.; Staroverov, V. N.; Keith, T.; Kobayashi, R.; Normand, J.; Raghavachari, K.; Rendell, A.; Burant, J. C.; Iyengar, S. S.; Tomasi, J.; Cossi, M.; Millam, J. M.; Klene, M.; Adamo, C.; Cammi, R.; Ochterski, J. W.; Martin, R. L.; Morokuma, K.; Farkas, O.; Foresman, J. B.; Fox, D. J. *Gaussian 16*; Gaussian, Inc.: Wallingford, CT, 2016.
(53) Klippenstein, S. J.; Wagner, A. F.; Dunbar, R. C.; Wardlaw, D. M.; Robertson, S. H.. *VARIFLEX*, version 1.00, 1999.
(54) Barker, J. R.; Nguyen, T. L.; Stanton, J. F.; Aieta, C.; Ceotto, M.; Gabas, F.; Kumar, T. J. D.; Li, C. G.; Lohr, L. L.. et al.*Multiwell-2017.1 Software Suite*; J.R. Barker, University of Michigan: Ann Arbor, Michigan, 2017, http://claspresearch.engin.u-mich.edu/multiwell/.
(55) Eyring, H. The activated complex in chemical reactions. *J. Chem. Phys.* **1935**, *3*, 107−115.
(56) Klippenstein, S. J. Variational optimizations in the Rice−Ramsperger−Kassel−Marcus theory calculations for unimolecular dissociations with no reverse barrier. *J. Chem. Phys.* **1992**, *96*, 367−371.
(57) Klippenstein, S. J. A bond length reaction coordinate for unimolecular reactions. II. Microcanonical and canonical implementations with application to the dissociation of NCNO. *J. Chem. Phys.* **1991**, *94*, 6469−6482.
(58) Holbrook, K. A.; Pilling, M. J.; Robertson, S. H. *Unimolecular Reactions*; J. Wiley: Chichester, UK, 1996.
(59) Eckart, C. The penetration of a potential barrier by electrons. *Phys. Rev.* **1930**, *35*, 1303−1309.
(60) Miller, J. A.; Klippenstein, S. J. The recombination of propargyl radicals: Solving the master equation. *J. Phys. Chem. A* **2001**, *105*, 7254−7266.
(61) Hippler, H.; Troe, J.; Wendelken, H. J. Collisional deactivation of vibrationally highly excited polyatomic molecules. II. Direct observations for excited toluene. *J. Chem. Phys.* **1983**, *78*, 6709−6717.
(62) Mourits, F. M.; Rummens, F. H. A. A critical evaluation of Lennard−Jones and Stockmayer potential parameters and of some correlation methods. *Can. J. Chem.* **1977**, *55*, 3007−3020.
(63) Tardy, D. C.; Rabinovitch, B. S. Collisional Energy Transfer. Thermal Unimolecular Systems in the Low-Pressure Region. *J. Chem. Phys.* **1966**, *45*, 3720−3730.
(64) Yu, J.; Dong, S. H.; Sun, G. H. Series solutions of the Schrödinger equation with position-dependent mass for the Morse potential. *Phys. Lett. A* **2004**, *322*, 290−297.
(65) Alecu, I. M.; Gao, Y.; Hsieh, P.-C.; Sand, J. P.; Ors, A.; McLeod, A.; Marshall, P. Studies of the Kinetics and Thermochemistry of the Forward and Reverse Reaction Cl + C_6H_6 = HCl + C_6H_5. *J. Phys. Chem. A* **2007**, *111*, 3970−3976.
(66) Moskaleva, L. V.; Lin, M. C. Theoretical Study of the NH_2 + C_2H_2 Reaction. *J. Phys. Chem. A* **1998**, *102*, 4687−4693.
(67) Chase, M. W., Jr. *NIST-JANAF Thermochemical Tables*, 4th ed.; American Chemical Society−American Institute of Physics for the National Institute of Standards and Technology: Washington D. C.−Woodbury, New York, 1998.
(68) Hatton, W. E.; Hildenbrand, D. L.; Sinke, G. C.; Stull, D. R. Chemical Thermodynamic Properties of Aniline. *J. Chem. Eng. Data* **1962**, *7*, 229−231.
(69) Vriens, G. N.; Hill, A. G. Equilibria of several reactions of aromatic amines. *Ind. Eng. Chem.* **1952**, *44*, 2732−2735.
(70) Cole, L. G.; Gilbert, E. C. The heats of combustion of some nitrogen compounds and the apparent energy of the N-N bond. *J. Am. Chem. Soc.* **1951**, *73*, 5423−5427.
(71) Anderson, C. M.; Gilbert, E. C. The apparent energy of the N-N bond as calculated from heats of combustion. *J. Am. Chem. Soc.* **1942**, *64*, 2369−2372.
(72) Lemoult, M. P. Recherches theoriques et experimentales sur les chaleurs de combustion et de formation des composes organiques. *Ann. Chim. Phys.* **1907**, *12*, 395−432.

https://dx.doi.org/10.1021/acsomega.9b03967
ACS Omega 2020, 5, 1277−1286